Effects of a spin-polarized current assisted Ørsted field in magnetization patterning

Oleksii M. Volkov, Volodymyr P. Kravchuk, Denis D. Sheka, Yuri Gaididei, and Franz G. Mertens

---

Articles you may be interested in

Effect of Dzyaloshinskii-Moriya interaction on the magnetic vortex oscillator driven by spin-polarized current
J. Appl. Phys. **117**, 17B720 (2015); 10.1063/1.4915476

Reliable low-power control of ultrafast vortex-core switching with the selectivity in an array of vortex states by in-plane circular-rotational magnetic fields and spin-polarized currents
Appl. Phys. Lett. **92**, 022509 (2008); 10.1063/1.2807274

Effect of nanosize modulation of granular La 0.67 Sr 0.33 MnO 3 manganites on temperature-dependent low-field spin-polarized tunneling magnetoresistance
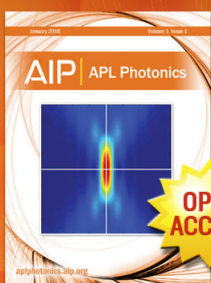J. Appl. Phys. **98**, 014306 (2005); 10.1063/1.1928307

Effect of the classical ampere field in micromagnetic computations of spin polarized current-driven magnetization processes
J. Appl. Phys. **97**, 10C713 (2005); 10.1063/1.1853291

Circular domain wall motion driven by spin-polarized currents in confined square nanomagnets
J. Appl. Phys. **97**, 044306 (2005); 10.1063/1.1847725

Effects of a spin-polarized current assisted Ørsted field in magnetization patterning

Oleksii M. Volkov,[1,a] Volodymyr P. Kravchuk,[2] Denis D. Sheka,[1] Yuri Gaididei,[2] and Franz G. Mertens[3]

[1]*Taras Shevchenko National University of Kiev, 01601 Kiev, Ukraine*
[2]*Bogolyubov Institute for Theoretical Physics, 03680 Kiev, Ukraine*
[3]*Physics Institute, University of Bayreuth, 95440 Bayreuth, Germany*

A spin-polarized electrical current leads to a variety of periodical magnetic structures in nanostripes. In the presence of the Ørsted field, which always assists an electrical current, the basic types of magnetic structures, i.e., a vortex-antivortex crystal and cross-tie domain walls, survive. The Ørsted field prevents saturation of the nanostripe and a longitudinal domain wall appears instead. Possible magnetization structures in stripes with different geometrical and material properties are studied numerically and analytically. © 2015 AIP Publishing LLC.
[http://dx.doi.org/10.1063/1.4921977]

I. INTRODUCTION

In recent years a magnetic waveguide, which consists of periodic magnetic structures, became an object of interest due to Bragg reflections which affect the spin wave dispersion. Magnetic waveguides can be fabricated by alternating material[1,2] or geometrical[3–6] parameters. All these magnetic waveguides are permanent, i.e., the spectra of spin waves cannot be changed dynamically after fabrication. However, it was demonstrated recently that using a strong spin-polarized current one can induce periodical magnetization structures on demand in nanomagnets.[7–10] These structures take the appropriate form according to the shape of the magnet and the current density: a square vortex–antivortex lattice is formed in a thin film,[7,8] a one-dimensional domain structure is formed in a nanowire,[9] and intermediate vortex-antivortex structures are formed in a thin stripe.[10] Such spin-current induced periodical magnetization structures can be used for dynamic control of the spin wave spectra in low-power filters and in other magnonic devices.[11]

There are two main techniques which allow to inject a pure spin-polarized current into a magnetic sample without creation of the current induced Ørsted field and significant heating. One of them utilizes geometrically separated areas with charge and spin currents injection and this technique is called non-local spin-current injection.[12–17] Another method utilizes spin-orbit torques which appear on the interconnection area of a ferromagnetic stripe and a nonmagnetic conductive layer with strong spin-orbit interactions. Using these spin-orbit torques, one can create different realizations of the classical field-like torque (e.g., indirect Rashba effect) and the Slonczewski-Berger torque (e.g., spin Hall effects and the direct Rashba effect).[17–19]

However, the simplest method of the spin-polarized current production is based on passing conducting electrons through a pillar magnetic heterostructure, see Fig. 1(a). In this method, the spin-polarized current is always assisted by

an Ørsted field, the exact form of which depends on the cross-section of the heterostructure. The pillar structure consists of two ferromagnetic layers (Polarizer and Sample) and a nonmagnetic Spacer between them, see Fig. 1(a). When the electrical current passes through the Polarizer the conduction electrons become partially spin-polarized in a direction, which is determined by the Polarizer magnetization. The Polarizer is usually made of a hard ferromagnetic material whose magnetization is kept fixed. The Spacer is produced from a nonmagnetic material which prevents the exchange and the dipole-dipole interactions between Polarizer and Sample. In a recent paper,[20] it was shown that the Spacer plays an important role in the process of spin diffusion due to interface scattering effects which result in a polarization change. However, for the sake of simplicity in our phenomenological study, we consider only thin and smooth interfaces between all layers. Thus, the spin-polarized electrons transfer the spin-torque from Polarizer to the Sample which can result in dynamics of the Sample magnetization. The spin-torque influence can be described phenomenologically by adding the Slonczewski-Berger torque to the Landau-Lifshitz equation.[21–23]
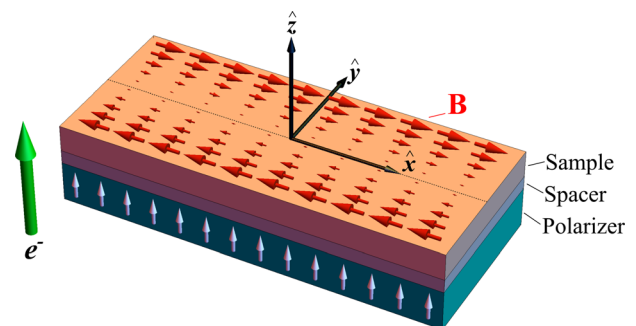

FIG. 1. The three-layer stripe-shaped spin valve. The spin polarized current flows perpendicularly to the studied stripe opposite to the $\hat{z}$–direction, thereby the conduction electrons flow to the opposite side, as shown by the green (large) arrow. The direction of polarizer magnetization and the Ørsted field distribution for a quasi-infinite stripe sample are indicated by small white and red arrows, respectively.

a)Electronic mail: alexey@volkov.ca

The aim of this work is to show that periodical structures can be formed in the case of action of a transverse spin-polarized current assisted by the Ørsted field on long ferromagnetic nanostripes. In our study, we consider two different spatial distributions of the Ørsted field: for stripes with infinite and finite length, see Figs. 1 and 8(a), respectively. By varying the stripe width, we study the current induced magnetization behavior in a wide range, starting from narrow stripes ($w \ll h$) and up to quasi two-dimensional wide stripes ($w \gg h$), where w and h denote the stripe width and thickness, respectively. We assume that the stripe is sufficiently long, so that $L \gg w$ and $L \gg h$ with L being the stripe length, and thin enough to ensure uniformity of the magnetization along the thickness. Details of the problem geometry are shown in Fig. 1.

II. MODEL DESCRIPTION

Our study is based on the Landau–Lifshitz–Slonczewski phenomenological equation[21–23]

$$\dot{\boldsymbol{m}} = \boldsymbol{m} \times \frac{\delta \mathcal{E}}{\delta \boldsymbol{m}} - j\alpha \frac{\boldsymbol{m} \times [\boldsymbol{m} \times \hat{z}]}{1 + \beta(\boldsymbol{m} \cdot \hat{z})}, \qquad (1)$$

where $\boldsymbol{m} = \boldsymbol{M}/M_s = (m_x, m_y, m_z)$ is the normalized magnetization vector, M_s is the saturation magnetization. The overdot indicates a derivative with respect to the rescaled time which is measured in units $(4\pi\gamma M_s)^{-1}$, γ is a gyromagnetic ratio, and $\mathcal{E} = E/(4\pi M_s^2)$ is the normalized magnetic energy. The normalized spin–current density $j = J/J_0$, where $J_0 = 4\pi M_s^2 |e|h/\hbar$, with e being the electron charge, $\hbar$ is the Planck constant. The spin–transfer torque efficiency coefficients α and β have the forms $\alpha = P\Lambda^2/[\Lambda^2 + 1]$ and $\beta = [\Lambda^2 - 1]/[\Lambda^2 + 1]$, where P is the degree of spin polarization, and the parameter Λ describes the resistance mismatch between the spacer and the ferromagnet stripe.[23,24] The damping is omitted in Eq. (1), because, as it was shown earlier,[8,9] the transverse spin–polarized current plays the role of an effective damping, which is usually greater than the natural one. It should also be noted that Eq. (1) is written for the case when the Polarizer is magnetized along the $\hat{z}$-axis, see Fig. 1.

We consider here a magnetic system, the total energy $E = E_{ex} + E_d + E_z$ of which consists of three parts: exchange, dipole-dipole, and Zeeman contributions. The exchange energy has the form

$$E_{ex} = A \int_V d\boldsymbol{r} \left[(\nabla m_x)^2 + (\nabla m_y)^2 + (\nabla m_z)^2 \right], \qquad (2)$$

where A is the exchange constant.

The energy of the dipole-dipole interaction is

$$E_d = \frac{M_s^2}{2} \int_V d\boldsymbol{r} \int_V d\boldsymbol{r}' \, (\boldsymbol{m}(\boldsymbol{r}) \cdot \nabla)(\boldsymbol{m}(\boldsymbol{r}') \cdot \nabla') \frac{1}{|\boldsymbol{r} - \boldsymbol{r}'|}. \qquad (3)$$

The Zeeman energy describes the interaction of the magnetic film with the Ørsted field $\boldsymbol{B}(J, \boldsymbol{r})$

$$E_z = -M_s \int_V d\boldsymbol{r} \, \boldsymbol{B}(J, \boldsymbol{r}) \cdot \boldsymbol{m}, \qquad (4)$$

where the spatial distribution of $\boldsymbol{B}(J, \boldsymbol{r})$ is determined by the form of the sample cross-section.

III. SIMULATION RESULTS

Here, we report on the results of a numerical study which is based on micromagnetic simulations.[25,26,33] The lengths of all studied stripes are the same $L = 1\,\mu m$. To ensure the magnetization uniformity along the $\hat{z}$-axis, we consider only thin stripes with a thickness of about one magnetic length, namely, $h = 5\,nm$. Since the thickness is small, the current density is assumed to be spatially uniform. The width is varied in a wide range $1 \leq w \leq 100\,nm$. A uniform in-plane magnetization state along the stripe (along the $\hat{x}$–axis) is chosen as an initial state for each simulation because it is very close to the ground state of a long stripe. In order to consider all possible current values, we adiabatically increase the current density from zero to values where the magnetization state does not depend on the current density.[27]

One has to stress that periodical magnetization structures appear just below the saturation current $J_s \propto hM_s^2$.[8,9] Therefore, there are two ways to decrease the saturation current density: (i) to use samples with smaller thickness, that is why in the current paper we consider thin stripes with $h = 5\,nm$, (ii) to use materials with smaller saturation magnetization. Therefore, we additionally carried out simulations for Nickel (Ni) stripes, namely, $M_s^{Ni} = 4.85 \times 10^5$ A/m versus $M_s^{Py} = 8.6 \times 10^5$ A/m. These results are presented in Appendix A.

Two different types of numerical experiments are performed by means of micromagnetic simulations. In the first type of simulations, we consider finite length stripe samples under the action of a pure spin-polarized current (without Ørsted field). As a result, we obtain all magnetization states which were found in our previous studies for thicker samples.[10] However, due to the thickness reducing from $h = 10\,nm$ in the previous simulations to $h = 5\,nm$ in the current ones, the typical current value, which corresponds to a certain magnetization state, becomes smaller. Namely, this current is nearly three times smaller for the same stripe width, see Figs. 2(a) and 2 in Ref. 10. Moreover, we perform the same simulations for stripes with periodic boundary conditions along the stripe, which models the quasi-infinite stripe sample. In these simulations, we do not find any principal differences with our previous results. This means that our stripe length $L = 1\,\mu m$ is large enough to generalize the phase diagram Fig. 2(a) for longer stripes.

In the second type of simulations, we consider quasi-infinite ferromagnetic stripe samples under the combined action of the spin-polarized current and the Ørsted field. In these simulations, we also use periodic boundary conditions along the stripe. In this case, the exact form of the field reads

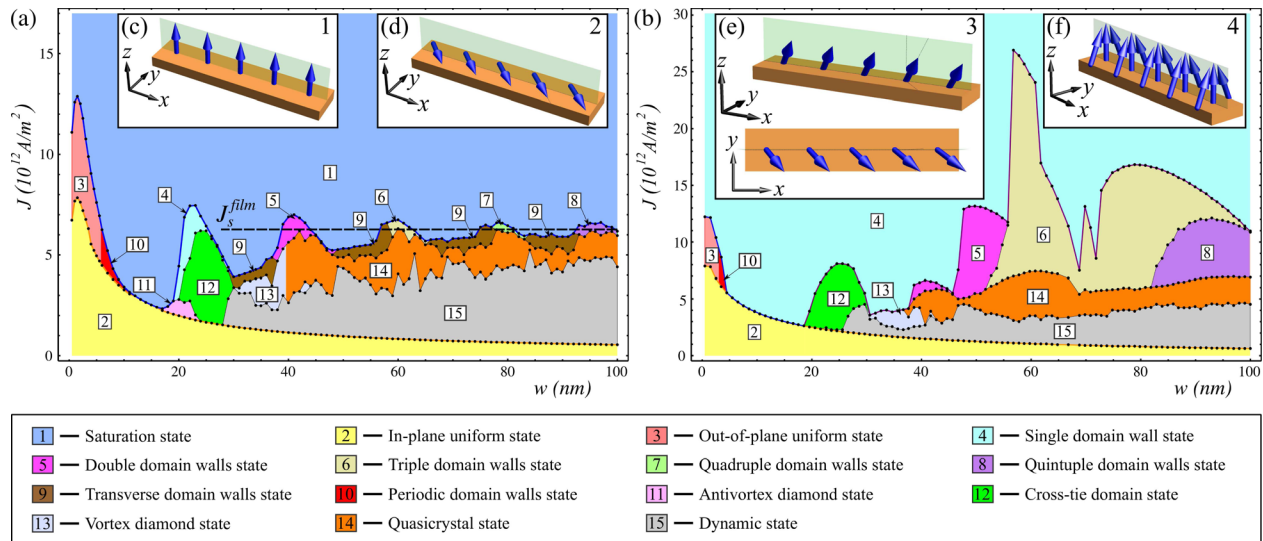$$\boldsymbol{B}(J, \boldsymbol{r}) = \frac{4\pi}{c} Jy\hat{x}, \qquad (5)$$

FIG. 2. The phase diagrams of the magnetization behavior of Py stripes of different widths w under the action of a transverse spin current J: (a) no Ørsted field, (b) Ørsted field is taken into account, see Fig. 1, and periodic boundary conditions are applied. Length $L = 1$ μm and thickness $h = 5$ nm of the stripes are fixed. Black bold dots indicate the transition from one state to another, and each state is numerated, in concordance with the legend. In the same way as in Fig. 2 of Ref. 10, states 10–14 show all possible periodical magnetization structures, and the inset pictures (c)–(e) show the possible uniform states: the saturation state, the in-plane and the out-of-plane uniform states, respectively. The inset picture (f) shows the single domain wall state.

where c is the speed of light. All possible types of the magnetization behavior in these micromagnetic simulations are summarized in the form of the phase diagram which is presented in Fig. 2(b).

Comparing the two diagrams in Fig. 2, one can conclude that the field influence is not significant for cases of narrow stripes and/or low current densities. This is due to the fact that the maximum value of the Ørsted field is directly proportional to the current density and the stripe width, $B_{max} \propto Jw/2$. In these cases, the same magnetization states appear: the uniform in-plane state for small current densities and for all stripe widths, see the region 2 of the phase diagrams in Fig. 2; the uniform out-of-plane state for narrow widths and higher current densities, see the region 3; the periodic domain structure (region 10). However, for the case of strong currents there is an important difference between these two cases: the action of the Ørsted field disables the saturation state and the single domain wall state appears instead of it, see the region 4 in Fig. 2(b) and the inset Fig. 2(f). This is the result of competition between influences of spin-torque and the Ørsted field on the magnetization and will be discussed in more details in Sec. IV.

For the intermediate values of the current density, there are observed the chaotic dynamical regime and stable periodic magnetization structures in both simulation cases: with and without Ørsted field. However, there are number of differences between these two regimes: (I) the vortex-antivortex quasicrystals, the cross-tie domain walls, and the vortex diamond states remain stable in both cases, although in stripes under the action of the Ørsted field the quasicrystals undergo a deformation; (II) the antivortex diamond state and the transverse domain wall states do not remain under the Ørsted field action; (III) in the case of the field absence a state with a single longitudinal domain wall appears only in a small region on the phase diagram between the saturated

and the cross-tie domain wall states, see region 4 in Fig. 2(a). Contrary to this, in the case of joint action of the spin-current assisted by the Ørsted field, a similar single domain wall state appears for any stripe width if the current is strong enough, see region 4 in Fig. 2(b); and (IV) the area of regions with multiple longitudinal domain walls increases significantly under the Ørsted field action.

We use the two-dimensional (2D) Fourier transform of the out-of-plane magnetization component

$$F_z^{2D}(\boldsymbol{k}_j) = \frac{1}{N_{xy}} \sum_{i=1}^{N_{xy}} \left[m_z(\boldsymbol{r}_i) - \langle m_z \rangle \right] e^{-i\boldsymbol{k}_j \boldsymbol{r}_i}, \qquad (6)$$

in order to distinguish and analyze various periodical structures, such as the longitudinal domain walls, the vortex-antivortex quasicrystals, and the cross-tie domain walls. In Eq. (6), N_{xy} is the total number of mesh cells in a square area where the Fourier transform is applied, $\boldsymbol{r}_i = (x_i, y_i)$ is a two-dimensional vector pointing to the appropriate cell, $\langle m_z \rangle = \frac{1}{N_{xy}} \sum_{i=1}^{N_{xy}} m_z(\boldsymbol{r}_i)$ is the averaged out-of-plane magnetization component, and $\boldsymbol{k}_j = (k_j^x, k_j^y)$ is a 2D wave vector. As one can conclude from Fig. 3(a), the action of the Ørsted field leads to the deformation of the quasicrystal state at stripe edges, this results in the formation of additional peaks in the 2D Fourier spectrum, see Fig. 3(a). For the case of the longitudinal domain wall, the k_x components are absent in the Fourier spectrum, see Fig. 3(b). This feature is used for the structure separation in the phase diagrams in Fig. 2. On the other hand, this feature allows us only to distinguish the two-dimensional and the one-dimensional magnetization structures, and it could not help in the separation of the magnetization structures with different numbers of domain walls, which take place on both diagrams, see Figs. 2(a) and 2(b). For this separation, we consider the distribution of the out-of-plane magnetization component m_z along the stripe width,
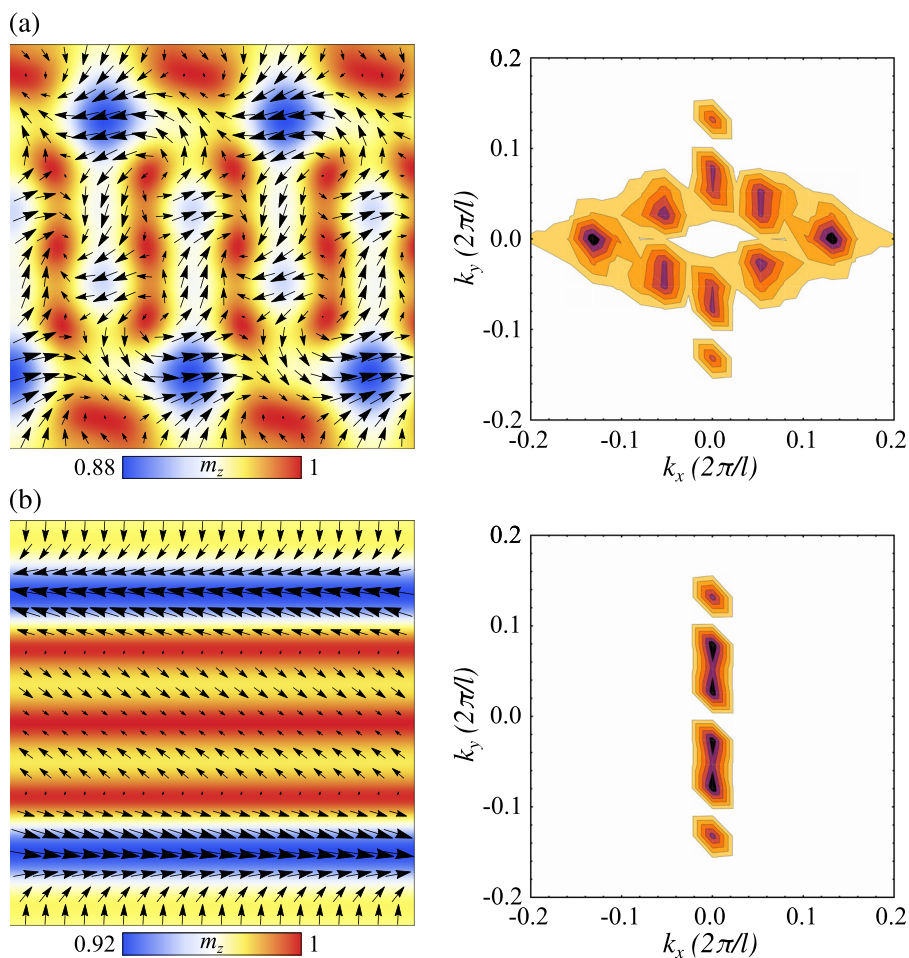
FIG. 3. Magnetization distributions and its two-dimension Fourier spectra of the square central part of the stripe with $w = 93$ nm width with quasi-crystal magnetization state (a) and quintuple domain wall state (b), which were obtained for currents $J = 6 \times 10^{12}$ A/m^2 and $J = 7 \times 10^{12}$ A/m^2, respectively. The wave vector components k_x and k_y are measured in units $2\pi/\ell$, where ℓ is the exchange length.

and we count all maxima which appear on it. This number of maxima shows us the corresponding number of the domain walls, as one can see from the insets (a)–(c) in Fig. 4.

On the next stage of our study, we consider the dependence of the averaged out-of-plane magnetization component $\langle m_z \rangle$ on the current density for the stripe sample with $w = 93$ nm, as one can see from the upper panel in Fig. 4. Regions of various magnetization states are shown in a way how they appear during the current density increase: region 2 is the static homogeneous magnetization state within the plane of the stripe with $\langle m_z \rangle = 0$, it was described in detail in Ref. 9; region 15 is the chaotic dynamical state of a vortex-antivortex gas and leads to a noisiness of the $\langle m_z \rangle$ component, however, its magnitude grows with the current density; region 14 is the vortex-antivortex quasicrystal state, which was described in detail in Ref. 8. For this current densities, the $\langle m_z \rangle(J)$ dependence becomes smooth but not monotonous. The existence of maxima is associated with the quasicrystal structure reorganization, which occurs with the growing of the current; regions 8, 6, and 4 are magnetization states with five, three, and one longitudinal domain walls, respectively. As one can see from Fig. 4, the $\langle m_z \rangle(J)$ dependence reaches its maximum in the region with five domain walls and after that it decreases smoothly with the increase of current density. During this process, the number of domain walls decreases to one. This happens due to the influence of the Ørsted field which becomes stronger with higher

values of current density and has the maximum magnitude on the stripe edges, see Fig. 1. As a final magnetization state, the single domain wall appears, it has its own characteristics: (i) in-plane magnetization components of the domain wall turn perpendicularly to the field, which is unusual, see the inset picture (a) in Fig. 5; (ii) the profile of the domain wall is described by a cosine with respect to the center of the stripe, see Fig. 5(b). It is different from the usual form of head-to-head or tail-to-tail domain walls in ferromagnetic samples which is described by a hyperbolic secant; (iii) in addition, the width of the domain wall Δw is determined by the stripe width and does not depend on the material parameters as for usual domain walls. (iv) For large current densities, the form of the domain wall becomes "frozen," in other words, it does not change during the current growing. To show the last characteristic, we consider the dependence of the domain wall Δw on the current density for the stripe sample with $w = 93$ nm width, see Fig. 5. The width Δw is found as a full width at half maximum for each current density, as is shown on the inset of Fig. 5(b). As one can see, this dependence reaches the maximum and, after that, it decreases reaching some horizontal asymptote. This means that for infinitely high currents an unchangeable structure appears which is analyzed in Sec. IV.

The maximum on the dependence in Fig. 5 can be explained as an influence of edge effects, which appear from the competition of the dipole-dipole interaction with the
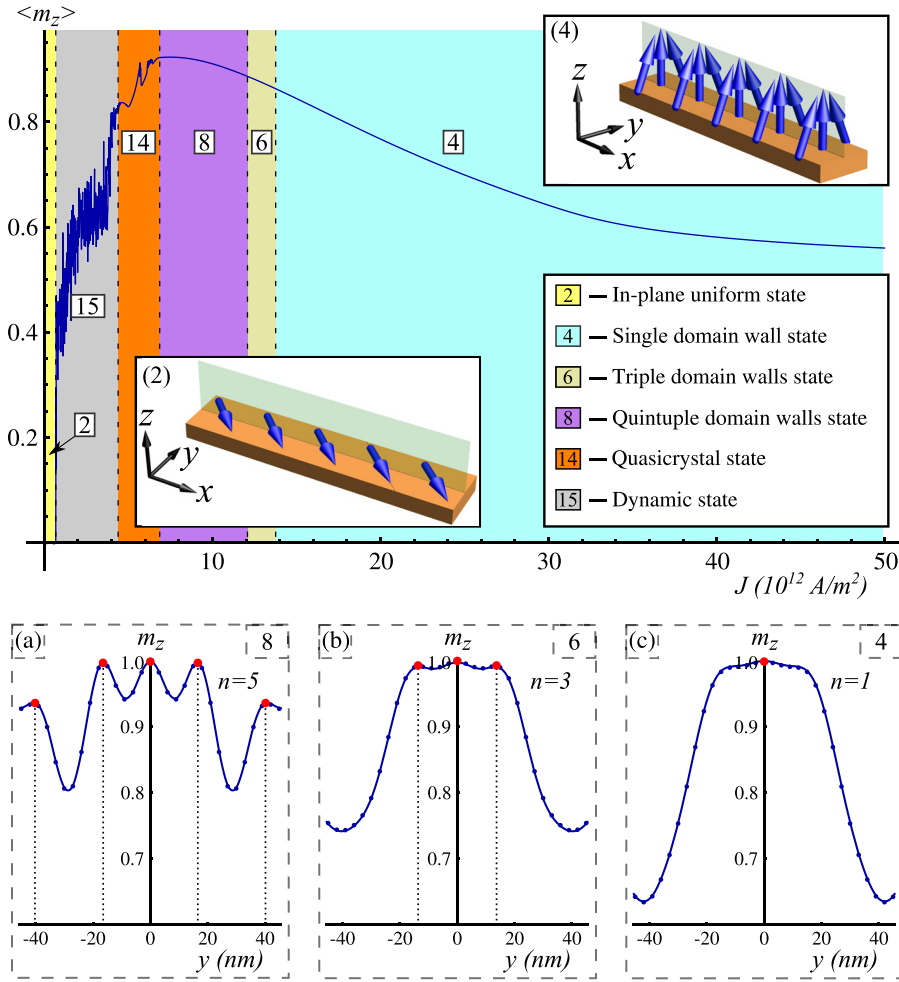
FIG. 4. Dependence of the average out-of-plane magnetization component $\langle m_z \rangle$ on the current density in the case of the quasi-infinite stripe with $w = 93$ nm. The row of panels (a)–(c) show the out-of-plane magnetization distributions along the stripe width for quintuple ($J = 7 \times 10^{12}$ A/m^2), triple ($J = 12.5 \times 10^{12}$ A/m^2), and single ($J = 15 \times 10^{12}$ A/m^2) longitudinal domain walls states, respectively.

current induced field and the spin-transfer torque on the stripe edge. The influence of the edge effects becomes even stronger when we study the action of the spin-current assisted Ørsted field on finite length stripe samples, see Appendix B for details.
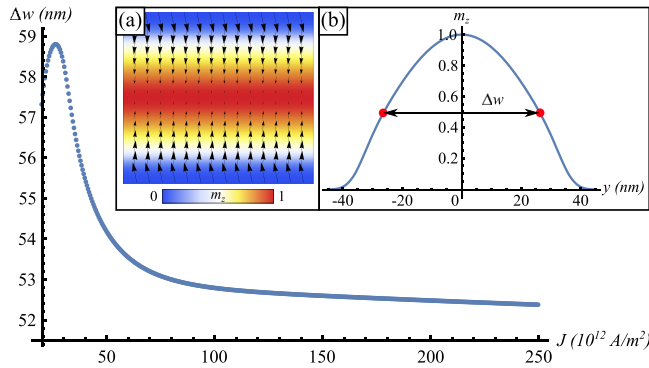

FIG. 5. Dependences of the domain wall width Δw on the current density for a quasi-infinite Py stripe with $w = 93$ nm for the case of combined action of the Ørsted field and the spin-polarized current. The inset picture (a) shows the in-plane magnetization distribution in the central area of the stripe with dimensions 100×93 nm^2 for the same current density. The inset picture (b) shows the out-of-plane magnetization distribution along the stripe width for $J = 250 \times 10^{12}$ A/m^2 and the definition of Δw.

IV. LONGITUDINAL DOMAIN WALL INDUCED BY STRONG CURRENT

In this section, we show that for strong current densities the competition of the Ørsted field and the spin-torques results in a formation of the single longitudinal domain wall instead of the uniformly saturated state. For qualitative description of the phenomenon, it is enough to model the magnetostatic energy of the stripe by the biaxial anisotropy[28–30]

$$E_{an}^{ef} = \frac{1}{2} \int_V d\boldsymbol{r} \left(K_p m_z^2 - K_a m_x^2 \right), \tag{7}$$

where $K_p > 0$ and $K_a > 0$ are easy-plane and easy-axis anisotropy coefficients, respectively, which can be assessed as demagnetization factors of a thin ferromagnetic stripe.[31]

Taking into account Eqs. (2), (4), (5), and (7) and using the representation of the magnetization vector in the spherical coordinate system $\boldsymbol{m} = (\sin\theta\cos\phi; \sin\theta\sin\phi; \cos\theta)$, one can get the corresponding total normalized energy of the system

$$\mathcal{E} = \frac{1}{2} \int_V d\boldsymbol{r} \Big\{ \ell^2 \big[(\nabla\theta)^2 + \sin^2\theta(\nabla\phi)^2 \big] + k_p \cos^2\theta$$
$$- k_a \sin^2\theta \cos^2\phi - 2j \frac{yh}{s_0} \sin\theta\cos\phi \Big\}, \tag{8}$$

where $k_p = \frac{K_p}{4\pi M_s^2}$ and $k_a = \frac{K_a}{4\pi M_s^2}$ are the normalized coefficients of effective anisotropy, $\ell = \sqrt{\frac{2A}{4\pi M_s^2}}$ is the exchange length, and $s_0 = \frac{\Phi_0}{\pi B_0}$ is an effective area, where $\Phi_0 = \hbar \pi c/|e|$ is the magnetic flux quantum and $B_0 = 4\pi M_s$ is the saturation field. For Permalloy $\ell \approx 5.3$ nm, $B_0 \approx 1.08 \times 10^4$ G, it is remarkable that the value of the effective area $s_0 \approx 6.09 \times 10^2$ nm^2 is of the same order of magnitude as the area of the stripe cross-section. Substituting the energy (8) into Eq. (1) and considering only static solutions, we obtain the set of equations

$$\ell^2 \nabla \left(\sin^2\theta \nabla\phi \right) - k_a \sin^2\theta \sin\phi \cos\phi$$
$$- j\sin\theta \left[\frac{yh}{s_0}\sin\phi + \frac{\alpha\sin\theta}{1+\beta\cos\theta} \right] = 0, \qquad (9a)$$

$$\ell^2 \Delta\theta + \frac{\sin 2\theta}{2}\left[k_p + k_a\cos^2\phi - \ell^2(\nabla\phi)^2 \right]$$
$$+ j\frac{yh}{s_0}\cos\theta\cos\phi = 0. \qquad (9b)$$

One can see that in the case of high current density $k_p, k_a \ll jyh/s_0$, there is a solution in a linear approximation

$$\theta \approx \frac{2}{P}\frac{h}{s_0}y, \qquad (10a)$$

$$\phi \approx -\frac{\pi}{2}. \qquad (10b)$$

The linear approximation in Eq. (10a) works well in the whole range of parameters $y \in (0, w/2)$ under the following condition:

$$c = \frac{w^2 h^2 \left(1 - \beta - 2\beta^2 \right)}{24\alpha^2 s_0^2} \ll 1. \qquad (11)$$

This means that one can neglect the next term in a series. For our material and geometrical parameters for a stripe sample with $w = 93$ nm $c \approx 0.08 \ll 1$, hence the linear dependence works well for all the range of $y \in (0, w/2)$.

The solution (10) originates from the competition of the spin-torque, which is created by the spin-polarized current and the influence of the Ørsted field. As one can see, the solution (10a) contains only geometrical and material parameters of the sample and does not include the current density. This fact means that for the high current densities we obtain a "frozen" single domain wall, whose form does not change with the increasing current. As one can see from Figs. 5 and 6, our analytical solutions (10) are in a good agreement with simulation data for strong enough currents

V. SUMMARY

We study numerically the periodical structures formation under the combined action of spin-polarized current and the current-induced Ørsted field in stripes with the two different Ørsted field distribution and different material parameters. We show that in all studied cases, cross-tie, longitudinal domain walls, and vortex-antivortex quasicrystals appear. As a result of the competition of the spin-polarized current and the Ørsted field, the single domain wall state appears instead of the saturation, which is obtained in the case of pure spin current without the Ørsted field. It is shown both numerically and analytically that the shape of this wall remains constant with the current increasing, and it depends only on geometrical and material parameters of the sample. The micromagnetic simulations confirm our analytical results with high accuracy. Also we show that periodic magnetization structures appear in different ferromagnetic materials and the required values of spin current can be reduced by utilizing materials with lower saturation magnetization, such as Nickel.

APPENDIX A: ACTION OF THE SPIN-CURRENT ASSISTED ØRSTED FIELD ON A NICKEL QUASI-INFINITE STRIPE

The aim of this Appendix is to show that utilizing materials with a smaller value of the saturation magnetization leads to a reduction of the current. For an example, we use
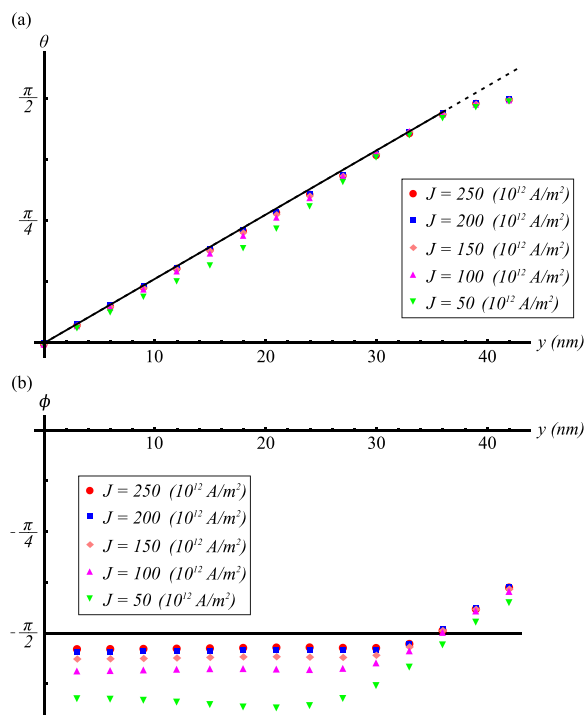

FIG. 6. Analytical solutions (10a) and (10b) for the single domain wall state (solid lines), compared to simulation data. Simulations were performed for a Permalloy stripe sample with width $w = 93$ nm.
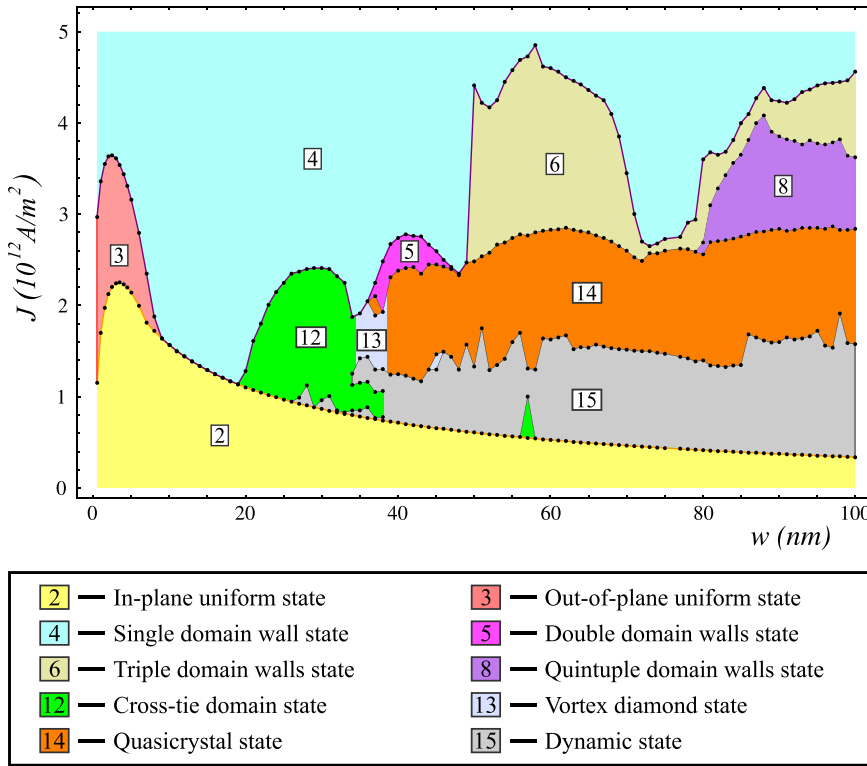
FIG. 7. The phase diagram of the magnetization behavior of Ni quasi-infinite stripes of different widths w under the co-action of the spin-polarized current and the assisted Ørsted field. The numeration of the magnetization states is the same as the numeration in Fig. 2.

2 — In-plane uniform state		3 — Out-of-plane uniform state	
4 — Single domain wall state		5 — Double domain walls state	
6 — Triple domain walls state		8 — Quintuple domain walls state	
12 — Cross-tie domain state		13 — Vortex diamond state	
14 — Quasicrystal state		15 — Dynamic state	

Ni quasi-infinite stripe samples. In this case, we take into account that Ni is a ferromagnetic material with cubic anisotropy and its total energy has the corresponding additional term

$$E_{an} = K_c \int_V d\mathbf{r} \, [m_x^2 m_y^2 + m_x^2 m_z^2 + m_y^2 m_z^2], \quad (A1)$$

where K_c is the cubic anisotropy coefficient.[32]

All simulation results are summarized in a phase diagram, which is shown in Fig. 7. By comparing results presented in Figs. 2(b) and 7, one can see that the critical current decreases by a factor of three.

APPENDIX B: THE COMBINED ACTION OF THE SPIN-POLARIZED CURRENT AND THE ØRSTED FIELD ON STRIPE SAMPLES WITH FINITE LENGTH

Here, we report on the results of the co-action of the spin-polarized current and the Ørsted field on stripe samples with finite length. The spatial distribution of the Ørsted field for the finite length stripe can be calculated by using the Biot–Savart law

$$\mathbf{B}(J, \mathbf{r}) = \frac{1}{c} \int_V d\mathbf{r}' \frac{\mathbf{J} \times (\mathbf{r} - \mathbf{r}')}{|\mathbf{r} - \mathbf{r}'|^3}, \quad (B1)$$

where J is the current density and $|\mathbf{r} - \mathbf{r}'| = \sqrt{(x - x')^2 + (y - y')^2 + (z - z')^2}$ with $\mathbf{r} = (x, y, z)$ and $\mathbf{r}' = (x', y', z')$. Doing an integration over the entire volume with $x' \in (-\frac{L}{2}, \frac{L}{2})$, $y' \in (-\frac{w}{2}, \frac{w}{2})$, and $z' \in (-\infty, \infty)$ and taking into account that the current flows through the ferromagnetic stripe in $-\hat{z}$-direction, while electrons are

moving in the opposite direction, it gives to us the magnetic field which can be written in the complex vector $\mathbf{B} = B_x + iB_y$ form

$$\mathbf{B}(J, \mathbf{r}) = \frac{2J}{c} \left\{ 2\pi y + \sum_{k=1}^{4} (-1)^k \xi_k^* \ln(\xi_k^*) \right\}, \quad (B2)$$

where $\ln(\xi_k) = \ln|\xi_k| + i \arg(\xi_k)$ is the complex logarithm, and $\{\xi_1 = (x + \frac{L}{2}) + i(y - \frac{w}{2}); \; \xi_2 = (x - \frac{L}{2}) + i(y - \frac{w}{2}); \; \xi_3 = (x - \frac{L}{2}) + i(y + \frac{w}{2}); \text{ and } \xi_4 = (x + \frac{L}{2}) + i(y + \frac{w}{2})\}$.

The final form of the Ørsted field distribution (B2) is described in Fig. 8(a). As one can see, the central part of the spatial field distribution is the same as the Ørsted field in the infinite length stripe; however, the rest parts are completely different, as one can see from Figs. 1 and 8(a), respectively.

As a result of the simulations, we obtain the phase diagram which is shown in Fig. 8(b). As one can see, the parts of the diagram which correspond to the narrow stripes and small current densities remain almost the same as they appear in the previous cases which are discussed in Sec. III and, similarly to the case of quasi-infinite stripes under the action of the spin-current and the Ørsted field, we also obtain the single domain wall state instead of the saturated one. In contrast to this, the parts of the diagram in Fig. 8(b) which correspond to wide stripes and large current densities are completely different from the same parts of the diagrams in Figs. 2(a) and 2(b). This occurs because the spatial distribution of the Ørsted field for finite length stripes leads to a strong influence of the edge effects in areas far from the center of the stripe. This edge effects start to play a key role in the processes of transition from one magnetization state to another: cross-tie domain walls appear instead of
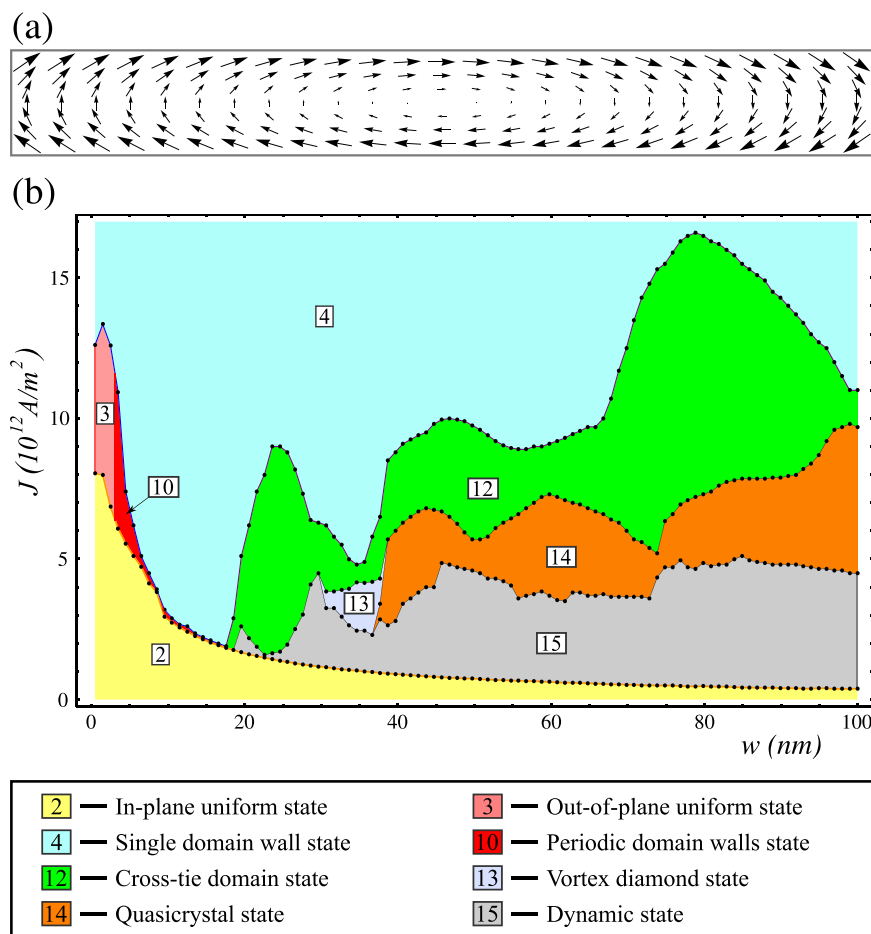
(a)

(b)

FIG. 8. (a) The spatial distribution of the Ørsted field induced by an electrical current within the finite stripe sample. (b) The phase diagram of the magnetization behavior of Py finite length stripes of different widths w under the co-action of the spin-polarized current and the Ørsted field, where all possible magnetization states have the same numeration as they have in Fig. 2.

2	— In-plane uniform state	3	— Out-of-plane uniform state
4	— Single domain wall state	10	— Periodic domain walls state
12	— Cross-tie domain state	13	— Vortex diamond state
14	— Quasicrystal state	15	— Dynamic state

longitudinal domain walls with the number of domains larger than one. At the same time, the magnetization structures, e.g., cross-tie domain wall state, vortex diamond state, and vortex-antivortex quasicrystals, remain stable, however, some of them undergo a deformation.

[1]Z. K. Wang, V. L. Zhang, H. S. Lim, S. C. Ng, M. H. Kuok, S. Jain, and A. O. Adeyeye, Appl. Phys. Lett. **94**, 083112 (2009).

[2]F. S. Ma, H. S. Lim, Z. K. Wang, S. N. Piramanayagam, S. C. Ng, and M. H. Kuok, Appl. Phys. Lett. **98**, 153107 (2011).

[3]A. V. Chumak, P. Pirro, A. A. Serga, M. P. Kostylev, R. L. Stamps, H. Schultheiss, K. Vogt, S. J. Hermsdoerfer, B. Laegel, P. A. Beck *et al.*, Appl. Phys. Lett. **95**, 262508 (2009).

[4]S.-K. Kim, K.-S. Lee, and D.-S. Han, Appl. Phys. Lett. **95**, 082507 (2009).

[5]K.-S. Lee, D.-S. Han, and S.-K. Kim, Phys. Rev. Lett. **102**, 127202 (2009).

[6]R. Huber, T. Schwarze, and D. Grundler, Phys. Rev. B **88**, 100405(R) (2013).

[7]O. M. Volkov, V. P. Kravchuk, D. D. Sheka, and Y. Gaididei, Phys. Rev. B **84**, 052404 (2011).

[8]Y. Gaididei, O. M. Volkov, V. P. Kravchuk, and D. D. Sheka, Phys. Rev. B **86**, 144401 (2012).

[9]V. P. Kravchuk, O. M. Volkov, D. D. Sheka, and Y. Gaididei, Phys. Rev. B **87**, 224402 (2013).

[10]O. M. Volkov, V. P. Kravchuk, D. D. Sheka, F. G. Mertens, and Y. Gaididei, Appl. Phys. Lett. **103**, 222401 (2013).

[11]Q. Wang, H. Zhang, X. Tang, H. Fangohr, F. Bai, and Z. Zhong, Appl. Phys. Lett. **105**, 112409 (2014).

[12]F. J. Jedema, A. T. Filip, and B. J. van Wees, Nature **410**, 345 (2001).

[13]F. J. Jedema, H. B. Heersche, A. T. Filip, J. J. A. Baselmans, and B. J. van Wees, Nature **416**, 713 (2002).

[14]D. Ilgaz, J. Nievendick, L. Heyne, D. Backes, J. Rhensius, T. A. Moore, M. Á. Niño, A. Locatelli, T. O. Menteş, A. V. Schmidsfeld, A. V. Bieren,

S. Krzyk, L. J. Heyderman, and M. Kläui, Phys. Rev. Lett. **105**, 076601 (2010); e-print arXiv:1008.2773 [cond-mat.mes-hall].

[15]T. Jungwirth, J. Wunderlich, and K. Olejnik, Nat. Mater. **11**, 382 (2012).

[16]N. Motzko, B. Burkhardt, N. Richter, R. Reeve, P. Laczkowski, W. Savero Torres, L. Vila, J.-P. Attané, and M. Kläui, Phys. Rev. B **88**, 214405 (2013).

[17]S. Takahashi and S. Maekawa, Sci. Technol. Adv. Mater. **9**, 014105 (2008).

[18]D. Wei, Y. Niimi, B. Gu, T. Ziman, S. Maekawa, and Y. Otani, Nat. Commun. **3**, 1058 (2012).

[19]A. V. Khvalkovskiy, V. Cros, D. Apalkov, V. Nikitin, M. Krounbi, K. A. Zvezdin, A. Anane, J. Grollier, and A. Fert, Phys. Rev. B **87**, 020402 (2013).

[20]C. Abert, G. Hrkac, M. Page, D. Praetorius, M. Ruggeri, and D. Suess, Comput. Math. Appl. **68**, 639–654 (2014).

[21]J. C. Slonczewski, J. Magn. Magn. Mater. **159**, L1 (1996).

[22]L. Berger, Phys. Rev. B **54**, 9353 (1996).

[23]J. C. Slonczewski, J. Magn. Magn. Mater. **247**, 324 (2002).

[24]V. Sluka, A. Kákay, A. M. Deac, D. E. Bürgler, R. Hertel, and C. M. Schneider, J. Phys. D: Appl. Phys. **44**, 384002 (2011).

[25]We use the OOMMF code, version 1.2a5. Size of the mesh cell is $3 \times X \times h$ nm^3, where X took values in the interval from 0.5 to 3 nm, depending on the stripe width. The width is changed with steps $\Delta w = 1$ nm for all samples. The current parameters are the following: polarization degree P $= 0.4$ and $\Lambda = 2$.

[26]M. J. Donahue and D. G. Porter, "OOMMF user's guide, version 1.0," Technical Report (Interagency Report NISTIR 6376, 1999).

[27]Density of the applied current is changed accordingly to the law: $J = t \, \Delta J / \Delta t$, where $\Delta J = 10^{10}$ A/m^2 and $\Delta t = 1$ ns. As a criterion of the saturation, we use the relation $M_z/M_s > 0.99$, where Mz is the total magnetization along the $\hat{z}$–axis.

[28]A. Thiaville, Y. Nakatani, J. Miltat, and N. Vernier, J. Appl. Phys. **95**, 7049 (2004).

[29]A. Thiaville, Y. Nakatani, J. Miltat, and Y. Suzuki, Europhys. Lett. (EPL) **69**, 990 (2005).

[30]A. Mougin, M. Cormier, J. P. Adam, P. J. Metaxas, and J. Ferré, EPL (Europhys. Lett.) **78**, 57007 (2007).

[31]A. Hubert and R. Schäfer, *Magnetic Domains: The Analysis of Magnetic Microstructures* (Springer–Verlag, Berlin, 1998).

[32]Nickel (Ni) material parameters: saturation magnetization $M_s = 4.85 \times 10^5$ A/m, exchange constant $A = 3.4 \times 10^{-12}$ J/m, constant of cubic anisotropy $K_c = -5.7 \times 10^3$ J/m^3 and exchange length $\ell = \sqrt{2A/(4\pi M_s^2)} = 4.8$ nm.

[33]Permalloy (Py, Ni$_{81}$Fe$_{19}$) material parameters: saturation magnetization $M_s = 8.6 \times 10^5$ A/m, exchange constant $A = 13 \times 10^{-12}$ J/m, exchange length $\ell = \sqrt{2A/(4\pi M_s^2)} = 5.3$ nm, and anisotropy is neglected.